Ab initio study on the anisotropy of mechanical behavior and deformation mechanism for boron carbide*

Jun Li(李君)[1], Shuang Xu(徐爽)[1], Jin-Yong Zhang(张金咏)[2], Li-Sheng Liu(刘立胜)[2,†], Qi-Wen Liu(刘齐文)[1], Wu-Chang She(佘武昌)[1], and Zheng-Yi Fu(傅正义)[2]

[1] *School of Science, Wuhan University of Technology, Wuhan* 430070, *China*

[2] *State Key Laboratory of Advanced Technology for Materials Synthesis and Processing, Wuhan University of Technology, Wuhan* 430070, *China*

(Received 24 November 2016; revised manuscript received 5 January 2017; published online 20 February 2017)

The mechanical properties and deformation mechanisms of boron carbide under *a*-axis and *c*-axis uniaxial compression are investigated by *ab initio* calculations based on the density functional theory. Strong anisotropy is observed. Under *a*-axis and *c*-axis compression, the maximum stresses are 89.0 GPa and 172.2 GPa respectively. Under *a*-axis compression, the destruction of icosahedra results in the unrecoverable deformation, while under *c*-axis compression, the main deformation mechanism is the formation of new bonds between the boron atoms in the three-atom chains and the equatorial boron atoms in the neighboring icosahedra.

Keywords: anisotropy, *ab initio* calculation, mechanical property, deformation mechanism

PACS: 71.15.Mb, 62.20.–x, 62.20.F– **DOI:** 10.1088/1674-1056/26/4/047101

1. Introduction

Boron carbide (B_4C) has wide industrial and military applications due to its excellent properties, including high hardness, low density and good chemical stability.[1–3] With a low density and high Hugoniot elastic limit (HEL) of about 20 GPa,[4,5] B_4C is expected to be a promising material for protective armor. However, when impact pressure is above HEL, an abrupt drop in strength occurs, leading to much poorer dynamics performance than expected.[5]

Since the 1990s, a number of groups have studied the mechanical behavior and related deformation mechanism experimentally.[4–10] Chen *et al.*[6] studied the formation of nanoscale intragranular amorphous bands in a ballistic experiment, which might be responsible for the lower dynamics response of B_4C. Amorphization of B_4C was also observed in scratching and indentation experiments.[7–10] By contrast, Zhang *et al.*[4] performed shock-wave experiments on B_4C, and found a sudden drop in the pressure-density plot above 38 GPa. They pointed out that it is related to a phase transition. Similarly, using plate impact experiments including reshock and release configurations, Vogler *et al.*[5] found that a possible structural change occurs at about 40 GPa. However, it is still difficult to analyze the failure mechanism in B_4C experimentally because of its complex crystal structure and the nearly identical scattering cross sections for neutron and electron of B and C.

Over the past few decades, *ab initio* methods based on the density functional theory have been widely used to study mechanical behaviors, deformation mechanisms and various properties in crystalline materials.[11–14] In particular, several theoretical studies in B_4C have been performed.[14–20] An *et al.*[14,15] considered the structure deformation mechanism under shear stress. They found that the amorphization band formation is associated with the breaking of B–C bond between neighboring icosahedra and the bond formation between the B atoms in the chain center and the C atoms in the nearby icosahedra.[14] They also concluded that the brittle failure of B_4C arises from the formation of higher density amorphous bands due to the fracture of the icosahedra through reactive molecular dynamics (RMD) simulations.[15] Besides, Aryal *et al.*,[16] Yan *et al.*,[17] and Taylor *et al.*[18,19] investigated the nature of structural deformation in B_4C under *c*-axis (the direction of three-atom chains) compression. They concluded that the deformation mechanism of B_4C is the abrupt bending of three-atom chains. Betranhandy *et al.*[20] suggested that the formation of C–C bonds in the C–B–C chains results in the dynamic failure of B_4C instead of the abrupt bending of C–B–C chains under the *c*-axis compression. Most of the above studies focused on the deformation mechanism of B_4C under the *c*-axis compression. The deformation behaviors for B_4C loading along other directions have not been understood.

Furthermore, Clellan *et al.*[21] showed experimentally that B_4C is more strongly anisotropic in elasticity and interatomic bonding than most solids. Thus, it needs to be considered whether the deformation mechanism for B_4C has strong anisotropy. Korotaev *et al.*[22] studied the structural changes in

*Project supported by the Science Fund from the Ministry of Science and Technology of China (Grant No. 2015DFR50650), the National Natural Science Foundation of China (Grant Nos. 51521001, 51502220, and 11402183), and the Fundamental Research Funds for the Central Universities of China (Grant Nos. WUT: 2016-ZY-066 and WUT: 2015IA014).

†Corresponding author. E-mail: liulish@whut.edu.cn

© 2017 Chinese Physical Society and IOP Publishing Ltd

B_4C during compression along different directions (x, y, and z axes). The z axis is the direction of three-atom chains, and the x axis is chosen so that the edge of the unit cell containing the carbon atom lays in the (x,z) plane. They found three types of structural changes: abrupt and continuous bending of the three-atom chain, and the disordering of the structure. They concluded that B_4C has a strongly anisotropic deformation behavior, because sudden chain bending occurs along the x axis and in y axis and z axis of deformation only continuous bending of the chain occurs. Actually, the sudden bending of three-atom chains was also observed along the z-axis compression (the three-atom direction).[16–19] Thus, the reason Korotaev *et al.*[22] proposed for the anisotropy of B_4C might not be the real anisotropic deformation behaviors. Thus, the anisotropic mechanical behaviors and associated deformation mechanisms still need investigating.

In order to investigate the anisotropic deformation mechanism in B_4C, *ab initio* methods are used to study the uniaxial compression deformation along a axis and c axis in this work. The rest of this paper is organized as follows. In Section 2, we give the details about crystal structure and computation. In Section 3, we present the results and discussion, containing stress–strain relation and the analyses of deformation mechanisms under a-axis and c-axis compressions. In Section 4, we draw some conclusions from the present study.

2. Crystal structure and computation details

As illustrated in Fig. 1, the crystal structure of B_4C consists of 12-atom icosahedra located at vertices of a rhombohedral lattice and the three-atom chain (C–B–C) lying on the main diagonal location. This structure can also be described as a hexagonal lattice with its c axis along the body diagonal of the primitive rhombohedral cell. Within an individual icosahedron, there are two types of distinct sites: polar and equatorial. Atoms at the polar sites connect the icosahedra together and atoms at the equatorial sites form bonds between the icosahedra and three-atom chains. In the present study, the hexagonal unit cell of $B_{11}C^P$–CBC, in which $B_{11}C^P$ is the 12-atom icosahedron at polar sites and C–B–C is the 3-atom chain, is considered. This structure is generally accepted as the most stable form of B_4C.[23–25]

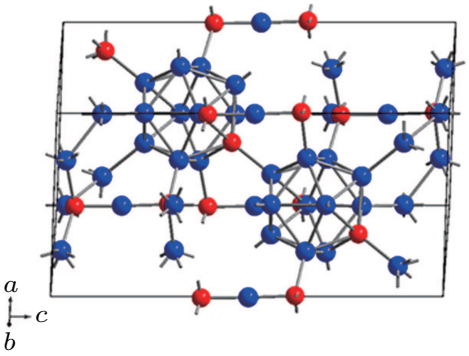


Fig. 1. (color online) Atomic structure of polar boron carbide $B_{11}C^P$–CBC in the hexagonal unit cells. The red balls in the figure denote the C atoms, and the blue balls refer to the B atoms.

In the current study, all periodic calculations were performed with an *ab initio* method at a local density approximation (LDA) functional level, and Vienna *ab initio* Simulation Package (VSA)[26–28] was used. To ensure accuracy and efficiency, tests were first made by using experimental unit cell parameters[29] of $B_{11}C^P$–CBC (Table 1) to determine the number of k-points and the cutoff energy required. According to the test results, 75 k-points and a high cutoff energy of 1200 eV were adopted in the present calculations. The convergence criteria were set to be 1×10^{-6} eV energy difference for solving the electronic wave function and 1×10^{-2} eV/Å force for geometry optimization. The lattice parameters for B_4C were first optimized in VASP to ensure that the calculations were based on equilibrium lattice parameters. The experimental lattice parameters (Table 1) were taken as the basis for the optimization by energy minimization. Due to the substitution of carbon into the B_{12} icosahedron, the $B_{11}C^P$–CBC structure rather deviates from hexagonal symmetry. Our optimized lattice parameters are listed in Table 1, which are in agreement with previous results.[16,30]

Table 1. Lattice parameters of $B_{11}C^P$–CBC.

Lattice parameters	Present work	Aryal *et al.*[16]	Ivashchenko *et al.*[30]	Morosin *et al.*[29]
a/Å	5.532	5.581	5.548	5.589
b/Å	5.532	5.581	5.548	5.589
c/Å	11.907	11.907	11.865	12.054
$\alpha/(^\circ)$	92.034	90.00	91.74	90
$\beta/(^\circ)$	87.966	92.075	88.26	90
$\gamma/(^\circ)$	119.887	120.055	119.89	120

In order to investigate the deformation mechanism of B_4C, the uniaxial compression along different directions were performed. The uniaxial compressive strains were imposed along a axis and c axis respectively. At each strain level, the strain components of the other directions were fully relaxed, and the residual stresses for relaxation of these other strain directions were controlled to be less than 0.1 GPa. To obtain stress–strain curves, a small uniaxial compression strain was

applied sequentially to the B_4C structure relaxed in the previous step. At each deformation step, we defined a 1% level of strain as a small compression strain increment. The volume of B_4C remained unchanged during relaxation. This stress–strain relationship was used to obtain mechanical behaviors and to analyze the related deformation mechanisms for B_4C.

3. Results and discussion

3.1. Stress–strain relationship

Figure 2 shows the uniaxial stress–strain responses for B_4C under uniaxial compressions. Under a-axis compression (Fig. 2(a)), the stress increases almost linearly until the strain reaches 0.12 ($\varepsilon = 0.12$). However, when the strain increases from 0.12 to 0.13, the stress decreases slightly from 66.4 GPa to 62.4 GPa. After $\varepsilon = 0.13$, the stress increases up to 89.0 GPa with a corresponding strain value of 0.22. After reaching a maximum value, the stress drops suddenly to a minimum value of −8.6 GPa, with a corresponding strain value of 0.23.

In Fig. 2, there are two abrupt points ($\varepsilon = 0.12$, $\varepsilon = 0.22$). In order to further investigate the mechanical behaviors relating to these two points, zoomed views of the regions near $\varepsilon = 0.12$ and $\varepsilon = 0.22$ are given. It is shown that the stress still varies linearly till $\varepsilon = 0.124$, while from $\varepsilon = 0.124$ to $\varepsilon = 0.126$, there is a slight decrease in stress from 68.2 GPa to 60.4 GPa. After that, the stress increases monotonically until reaching a maximum value. Beyond the point of maximum stress, the stress generally decreases monotonically. From $\varepsilon = 0.22$ to $\varepsilon = 0.224$, the stress decreases slightly from 89.0 GPa to 87.9 GPa. At $\varepsilon = 0.226$, there is a sudden drop in stress to 25.9 GPa. After that, the stress ultimately drops to a minimum value.

When compressive strains are imposed along the c axis (Fig. 2(b)), the mechanism is quite different. The stress increases almost linearly up to 168.8 GPa with a corresponding stain value of 0.22, indicating that the structure is uniformly resistant to the deformation. At $\varepsilon = 0.23$, an abrupt drop in stress to 14.2 GPa occurs. Zoomed views of the region near $\varepsilon = 0.22$ are also given in Fig. 2(b). The results show that the stress varies linearly to the maximum stress of 172.2 GPa with $\varepsilon = 0.228$.

The above results show that the maximum stress along a axis (89.0 GPa) is much smaller than that along the c axis (172.2 GPa). Thus the compressive strength along the c axis is higher than that along the a axis in the B_4C structure. However, the maximum stress that the B_4C can sustain is much larger than the experimental value.[4,5] That is because perfect crystal structure is considered in this work. But it is almost impossible to obtain the ideal compression conditions experimentally.

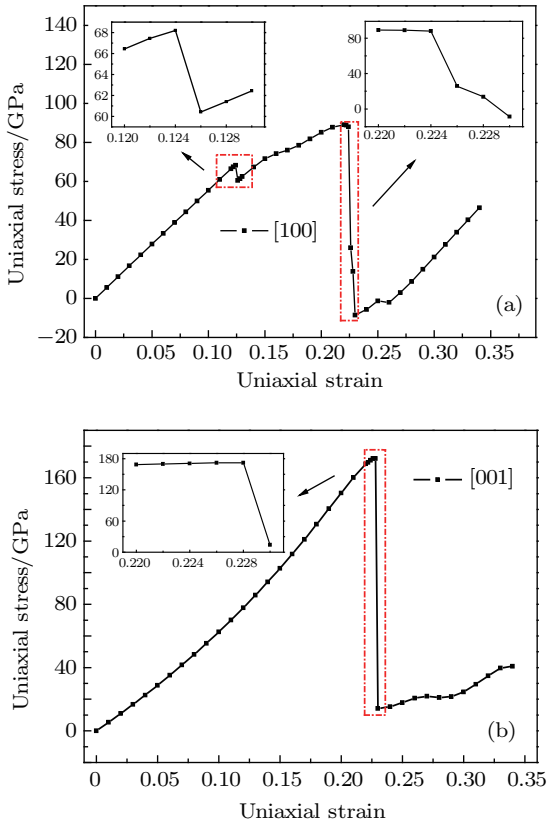


Fig. 2. (color online) Stress–strain relationships for B_4C under uniaxial compressions (a) a axis, (b) c axis.

From the above results, there are some differences between the mechanical behavior of the structure during compression along the a axis and that along the c axis. From $\varepsilon = 0.12$ to $\varepsilon = 0.13$, there is a slight decrease in stress under the compression along the a axis while the stress varies linearly under the compression along the c axis. Before reaching a minimum value, the stress decreases monotonically under the compression along the a axis while the stress drops suddenly under the compression along the c axis. These differences are mainly due to the anisotropy of B_4C. Thus the microstructure evolution of B_4C needs further studying, thereby clarifying the reasons why the mechanical behavior is anisotropic in B_4C under the a-axis and c-axis compressions.

3.2. Anisotropic deformation mechanism for B_4C

3.2.1. Compression along *a* axis

In other previous research,[16–19] the bending of three-atom chains was considered as the mechanism of B_4C under c-axis compression. In order to study whether the deformation mechanism of a axis is also related to the deformation of three-atom chains, the change in the angle of C–B–C chain with a-axis strain is shown in Fig. 3. Under the a-axis compression, the angle of C–B–C chain decreases monotonically

from 178.3° to 164.1° ($\varepsilon = 0.124$). Then a sudden decrease in angle associated with the bending of three-atom chains takes place, leading to a small decrease in stress from 68.2 GPa to 60.4 GPa in Fig. 2(a). From $\varepsilon = 0.126$ to $\varepsilon = 0.224$, the angle of C–B–C chain varies continuously. However, at $\varepsilon = 0.226$, the angle decreases suddenly. It is followed by an increase in the angle of C–B–C chain from 123.9° to 137.9° at $\varepsilon = 0.228$. At $\varepsilon = 0.23$, the angle of C–B–C chain actually rises slightly to 139.4°. From $\varepsilon = 0.22$ to $\varepsilon = 0.23$, the angle of C–B–C chain fluctuates up and down without any particular pattern. Thus, the bending of three-atom chains is not related to the deformation mechanism of a axis. As presented below, the electron localization function (ELF)[31–33] is further studied, which shows that the distortion of $B_{11}C^P$ icosahedron is the main reason for causing the stress to drop under the a-axis compression.

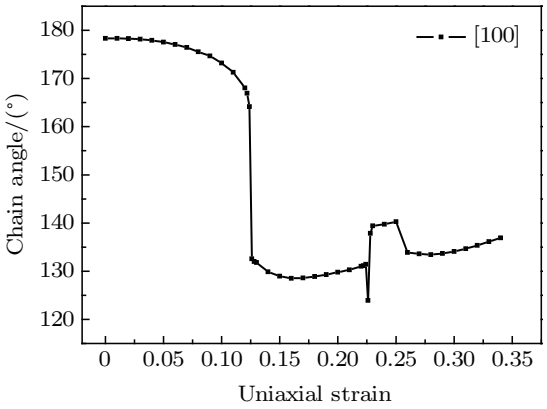


Fig. 3. Plot of angle of C–B–C chain versus uniaxial strain for B_4C under the a-axis compression.

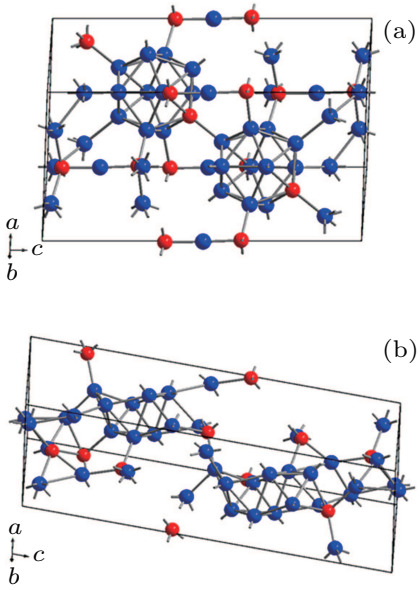


Fig. 4. (color online) Atomic configurations after unloading (a) $\varepsilon = 0.228$, (b) $\varepsilon = 0.23$ (blue = B atoms; red = C atoms).

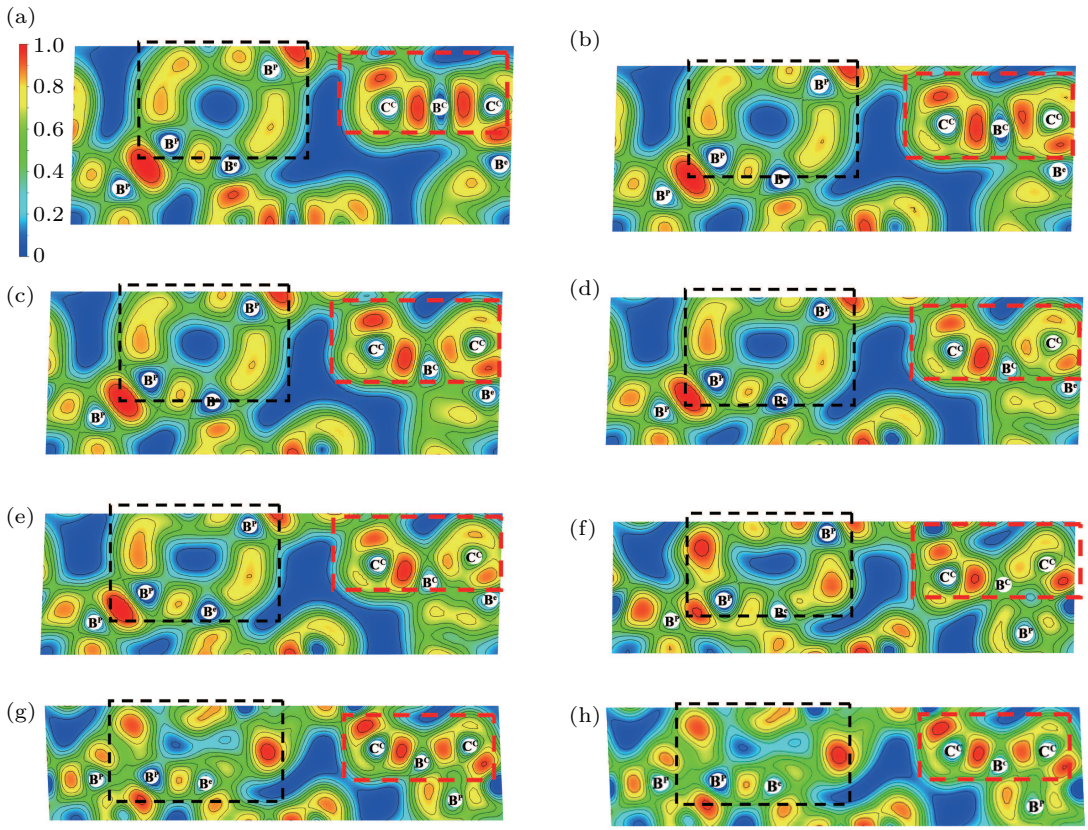


Fig. 5. (color online) Maps of the electron localization function (ELF) for uniaxial compression along the a axis at different strain levels in the plane containing the atoms in the chain (B^C and C^C) and boron polar (B^P) and equatorial (B^e) atoms of icosahedra. (a) $\varepsilon = 0.00$ corresponds to the initial stage, (b) $\varepsilon = 0.124$, (c) $\varepsilon = 0.126$ where the abrupt chain bending occurs but no extra bond is formed, (d) $\varepsilon = 0.22$, (e) $\varepsilon = 0.224$, (f) $\varepsilon = 0.228$ where the $B_{11}C^P$ icosahedra are highly distorted but still not broken, (g) $\varepsilon = 0.23$ where the icosahedra are broken, leading to the formation of some extra new bonds, and (h) $\varepsilon = 0.24$ corresponds to an unrecoverable deformation.

There are some discontinuous points in the stress–strain curve of B_4C under the *a*-axis compression. In order to further investigate the nature of deformation behaviors, we unload at different strain levels (between $\varepsilon = 0.126$ to $\varepsilon = 0.25$), then the typical atomic structures ($\varepsilon = 0.228$, $\varepsilon = 0.23$) are analyzed in detail as shown in Fig. 4. After unloading from $\varepsilon = 0.228$ (Fig. 4(a)), the crystal structure is the same as the original structure (Fig. 1), which means that the deformation of B_4C structure is still elastic as the strain increases from 0.126 to 0.228. While unloading from $\varepsilon = 0.23$ (Fig. 4(b)) and other higher strain levels, an unrecoverable deformation appears, which is mainly caused by the destruction of $B_{11}C^P$ icosahedra.

Figure 5 gives maps of the ELF which is used to analyze the covalent bonding and long pair formation.[31–33] Below $\varepsilon = 0.124$ (Figs. 5(a) and 5(b)), the three-atom chains are almost straight and the $B_{11}C^P$ icosahedra are intact. The B_4C structure uniformly resists the uniaxial deformation, leading to the monotonic increase in stress. At $\varepsilon = 0.126$ (Fig. 5(c)), an abrupt chain bending occurs (in the red dashed frame), leading to a small decrease in stress from 68.2 GPa to 60.4 GPa in Fig. 2(a). No extra bond formation is observed. As the applied strain increases to 0.224 (Figs. 5(d) and 5(e)), the C–B–C chains remain bent and the icosahedra are deformed slightly. At $\varepsilon = 0.228$ (Fig. 5(f)), the $B_{11}C^P$ icosahedra (in the black dashed frame) are highly distorted but still not broken, resulting in irregular fluctuation of the angle of C–B–C chain in Fig. 3. Actually, there is no bond broken nor formed. The B_4C structure is still in elastic deformation. The monotonic decrease in stress is mainly due to the distortion of $B_{11}C^P$ icosahedra. At $\varepsilon = 0.23$ (Fig. 5(g)), the icosahedra are broken, forming some extra new bonds. At the same time, an unrecoverable deformation occurs. As shown in Fig. 5(h), an unrecoverable deformation remains in the B_4C. The results indicate that when the chain bending occurs, the B_4C structure is still in elastic deformation stage, while the destruction of $B_{11}C^P$ icosahedra is the main reason for causing unrecoverable deformation.

3.2.2. Compression along *c* axis

Figure 6 shows the bending of C–B–C chains under the *c*-axis compression. Unlike the *a*-axis compression, the decrease in the angle of C–B–C chain is slower. When the strain is increased to 0.228, the angle changes slowly to 162.2°. After this point, there is an abrupt drop in the angle of C–B–C chain to 96.3°, which is related to the abrupt drop in stress.

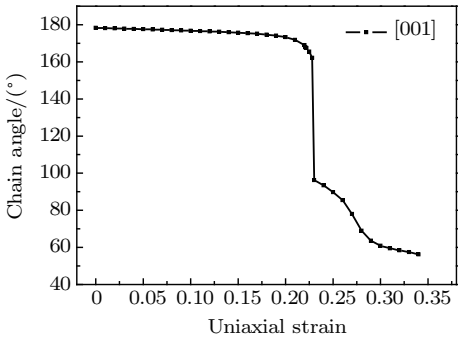


Fig. 6. Plot of angle of C–B–C chain versus uniaxial strain for B_4C under the *c*-axis compression.

The change in the angle of C–B–C chain during compression along the *a* axis is quite different from that along the *c* axis. Under *a*-axis compression, when the abrupt bending of C–B–C chains occurs, the stress decreases slightly from 68.2 GPa to 60.4 GPa. When the B_4C undergoes a stress drop, the fluctuation of angle of C–B–C chains appears. Meanwhile, under the *c*-axis compression, when the abrupt bending of C–B–C chains occurs, the stress drops suddenly from 172.2 GPa to 14.2 GPa.

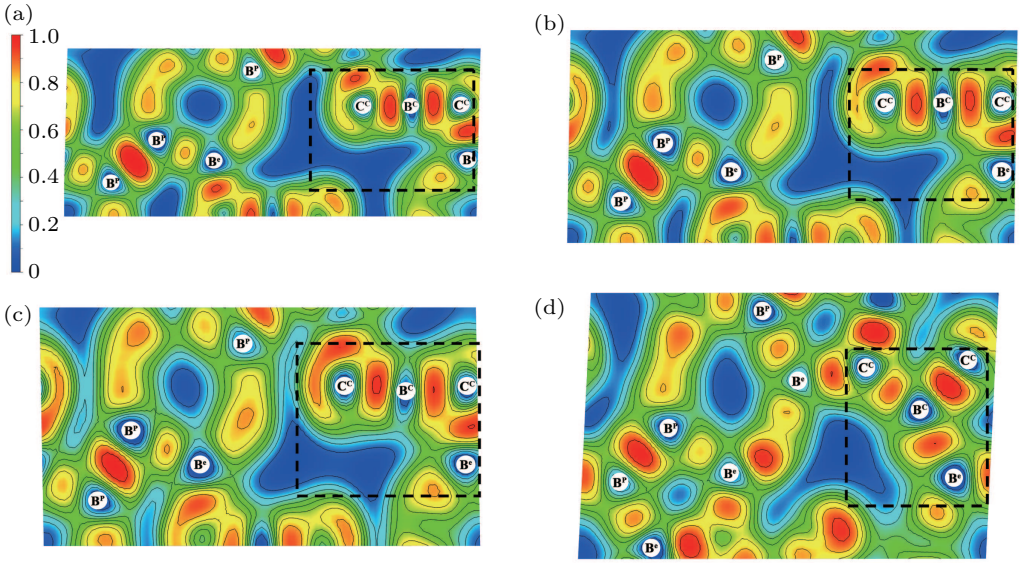


Fig. 7. (color online) Maps of the electron localization function (ELF) in the same plane as that in Fig. 5 for uniaxial compression along the *c* axis at (a) $\varepsilon = 0.00$ corresponds to the initial stage, (b) $\varepsilon = 0.13$ and (c) $\varepsilon = 0.228$ corresponds to the elastic deformation, (d) $\varepsilon = 0.23$ where the B atoms in the chain center make extra atomic bonds with the equatorial B atoms in neighboring deformed icosahedra, leading to the unrecoverable deformation.

Figure 7 displays maps of the ELF under the *c*-axis compression at different strains. Before $\varepsilon = 0.228$ (Figs. 7(a)–7(c)), all bonds vary continuously and there is no bond broken nor formed. The angle of three-atom chain is close to 180°. The $B_{11}C^P$ icosahedra are intact but deformed slightly. At $\varepsilon = 0.23$ (Fig. 7(d)), the B atoms in the chain center make extra atomic bonds with the equatorial B atoms in neighboring deformed icosahedra, leading to suddenly bending the C–B–C chains. The $B_{11}C^P$ icosahedra are still identifiable but severely disordered. So the formation of new atomic bonds between the B atoms in the middle of the chain and the equatorial B atoms in the neighboring deformed icosahedra is considered as the main mechanism for causing the stress to abruptly drop.

The strong anisotropy of deformation mechanism for B_4C is observed. Under the *a*-axis compression, when the sudden bending of C–B–C chains takes place, the stress drops slightly and the B_4C structure is still in the elastic stage. After that, the decrease in stress occurs, which is related to the distortion of B_4C structure, and the destruction of $B_{11}C^P$ icosahedra is the main mechanism for causing unrecoverable deformation. Under the *c*-axis compression, the formation of new atomic bonds between the B atoms in the middle of the chain and the equatorial B atoms in the neighboring deformed icosahedra is the main deformation mechanism, leading to an abrupt drop in stress.

4. Conclusions

In this work, *ab initio* methods are used to study the intrinsic mechanical properties and deformation mechanisms of B_4C under *a*-axis and *c*-axis compression. Strong anisotropy is observed. The maximum stresses are 89.0 GPa and 172.2 GPa along *a* axis and *c* axis, respectively. Under the *a*-axis compression, there is a slight decrease in the stress–strain curve, which is caused by the sudden bending of the C–B–C chains. However, the structure is still in elastic deformation at this time. Then the drop in stress takes place, which is associated with the distortion of B_4C structure, while the destruction of icosahedra is the main mechanism for causing the unrecoverable deformation. Under the *c*-axis compression, the icosahedra remain intact, and the C–B–C chains are almost straight before a drop in stress occurs. The formation of B–B bonds, which leads to the sudden bending of the C–B–C chains, is the main mechanism for causing the stress to abruptly drop.

References

[1] Domnich V, Reynaud S, Haber R A and Chhowalla M 2011 *J. Am. Ceram. Soc.* **94** 3605
[2] Lowther J E 2002 *Physica B: Condens. Matter* **322** 173
[3] Letsoalo T and Lowther J E 2008 *Physica B: Condens. Matter* **403** 2760
[4] Zhang Y, Mashimo T, Uemura Y, Uchino M, Kodama M, Shibata K, Fukuoka K, Kikuchi M, Kobayashi T and Sekine T 2006 *J. Appl. Phys.* **100** 113536
[5] Vogler T J, Reinhart W D and Chhabildas L C 2004 *J. Appl. Phys.* **95** 4173
[6] Chen M, McCauley J W and Hemker K J 2003 *Science* **299** 1563
[7] Ge D, Domnich V, Juliano T, Stach E A and Gogotsi Y 2004 *Acta Mater.* **52** 3921
[8] Chen M and McCauley J W 2006 *J. Appl. Phys.* **100** 123517
[9] Ghosh D, Subhash G, Lee C H and Yap Y K 2007 *Appl. Phys. Lett.* **91** 061910
[10] Domnich V, Gogotsi Y, Trenary M and Tanaka T 2002 *Appl. Phys. Lett.* **81** 3783
[11] Li X L, Wu P, Yang R, Yan D, Chen S, Zhang S and Chen N 2016 *Chin. Phys. B* **25** 036601
[12] Wang F, Lai W S, Li R S, He B and Li S F 2016 *Chin. Phys. B* **25** 066804
[13] Zhou P and He D W 2016 *Chin. Phys. B* **25** 017302
[14] An Q, Goddard W and Cheng T 2014 *Phys. Rev. Lett.* **113** 095501
[15] An Q and Goddard W A 2015 *Phys. Rev. Lett.* **115** 105501
[16] Aryal S, Rulis P and Ching W Y 2011 *Phys. Rev. B* **84** 184112
[17] Yan X Q, Tang Z, Zhang L, Guo J J, Jin C Q, Zhang Y, Goto T, McCauley J W and Chen M W 2009 *Phys. Rev. Lett.* **102** 075505
[18] Taylor D E, McCauley J W and Wright T W 2012 *J. Phys.: Condens. Matter* **24** 505402
[19] Taylor D E 2015 *J. Am. Ceram. Soc.* **98** 3308
[20] Betranhandy E, Vast N and Sjakste J 2012 *Solid State Sci.* **14** 1683
[21] Clellan K J M C, Chu F, Roper J M and Shindo I 2001 *J. Mater. Sci.* **36** 3403
[22] Korotaev P, Pokatashkin P and Yanilkin A 2016 *Comput. Mater. Sci.* **121** 106
[23] Lazzari R, Vast N, Besson J M, Baroni S and Corso A D 1999 *Phys. Rev. Lett.* **83** 3230
[24] Vast N, Lazzari R, Besson J M, Baroni S and Dal Corso A 2000 *Comput. Mater. Sci.* **17** 127
[25] Saal J E, Shang S and Liu Z K 2007 *Appl. Phys. Lett.* **91** 231915
[26] Kresse G and Furthmüller J 1996 *Comput. Mater. Sci.* **6** 15
[27] Kresse G and Furthmüller J 1996 *Phys. Rev. B* **54** 11169
[28] Kresse G 1999 *Phys. Rev. B* **59** 1758
[29] Morosin B, Kwei G H, Lawson A C, Aselage T L and Emin D 1995 *J. Alloys Compd.* **226** 121
[30] Ivashchenko V I, Shevchenko V I and Turchi P E A 2009 *Phys. Rev. B* **80** 235208
[31] Momma K and Izumi F 2011 *J. Appl. Crystallogr.* **44** 1272
[32] Becke A D and Edgecombe K E 1990 *J. Chem. Phys.* **92** 5397
[33] Silvi B and Savin A 1994 *Nature* **371** 683